Cent. Eur. J. Chem. • 11(5) • 2013 • 763-773
DOI: 10.2478/s11532-013-0207-6

VERSITA

Central European Journal of **Chemistry**

Facile synthesis of nanoscaled α-Fe_2O_3, CuO and CuO/Fe_2O_3 hybrid oxides and their electrocatalytic and photocatalytic properties

Research Article

Lu Pan[1,2*], Jing Tang[1], Fengwu Wang[1]

[1]*Department of Chemistry and Chemical Engineering, Huainan Normal University, Anhui, Huainan 232001, China*

[2]*Anhui Key Laboratory of Low temperature Co-fired Material, Huainan Normal University, Huainan 232001,China*

Received 9 October 2012; Accepted 3 January 2013

Abstract: A facile and easily controlled route was designed to synthesize nano-structured Fe_2O_3, CuO, and CuO/Fe_2O_3 hybrid oxides with different Cu/Fe molar ratios via a hydrothermal procedure. The samples were characterized by X-ray diffraction (XRD), X-ray photoelectron spectroscopy (XPS), transmission electron microscopy (TEM), high-resolution transmission electron microscopy (HR-TEM) and field-emission scanning electron microscopy (FE-SEM). The results showed that the morphologies of the samples changed with different Cu/Fe ratios. The electrocatalytic properties of the samples modified on a glassy carbon electrode for p-nitrophenol reduction in a basic solution were investigated. The results indicated that CuO/Fe_2O_3 hybrids with lower Cu/Fe ratio exhibited higher electrocatalytic activity. The photocatalytic performances of the samples for methyl orange degradation with assistance of oxydol under irradiation of visible light were studied. The results revealed that CuO/Fe_2O_3 hybrids with higher Cu/Fe ratio showed efficient photocatalytic activity.

Keywords: *CuO/Fe_2O_3 hybrid oxides • Electrocatalysis • Photocatalysis • p-nitrophenol • Methyl orange*

1. Introduction

Recent studies have shown that the physical and chemical properties of nanoscaled materials depend strongly on their structures, morphologies and compositions. Generally, the combination of two transition metals in an oxide matrix may produce new materials with novel chemical and physical properties that single one may not possess [1-4]. CuO and α-Fe_2O_3, two important transition metal oxides, have been studied and applied widely in many fields, including catalysts [5-8], sensors [9], water splitting [10], and water treatment [11-13]. In spite of the numerous reports of the single CuO or Fe_2O_3, CuO/Fe_2O_3 composites can exhibit much more excellent properties in many areas, such as catalysis [14-17], sensor [18], elctrochemistry [19], magnetism [20], *etc*. CuO/Fe_2O_3 composites have been synthesized with many methods, including solid phase reaction [14], hydrothermal [21], co-precipitation [17], sol-gel method [22], and so on. However, the reports on the synthesis of CuO/Fe_2O_3 oxides with different Cu/Fe molar ratios via a hydrothermal procedure are very limited. Herein we present a novel and easily controlled hydrothermal approach to synthesize pure Fe_2O_3, CuO, and CuO/Fe_2O_3 hybrid oxides with different Cu/Fe molar ratios. The present technique requires neither complicated steps nor template. Although CuO/Fe_2O_3 hybrids or composites have been used as catalysts frequently, to our best know, the report on the electrocatalytic performances using a cyclic voltammetry method can be referred rarely. In addition, single CuO or Fe_2O_3 nanaomaterial is often used as photocatalyst [23-28]. However, the report on the photocatalysis of CuO/Fe_2O_3 hybrids or composites is infrequent. In this work, the as-synthesized samples were used as electrocatalysts for *p*-nitrophenol reduction in a basic solution and as photocatalysts for degradation of methyl orange with assistance of oxydol under irradiation of visible light. The high catalytic activity of

* *E-mail: panlu1970 @163.com*

the samples suggested their potential application in electrocatalysis and photocatalysis in environmental treatment.

2. Experimental procedure

2.1. Materials

$NH_4Fe(SO_4)_2$•$12H_2O$, $CuSO_4$•$5H_2O$, cyclohexylamine, KC1, $K_3[Fe(CN)_6]$, $K_4[Fe(CN)_6]$, NaOH, methyl orange and *p*-nitrophenol, were purchased from Shanghai Chemical Reagent Co.(China). They were of analytic grade and used directly without any further treatment as received.

2.2. Synthesis of CuO/Fe_2O_3 samples

Typically, $NH_4Fe(SO_4)_2$•$12H_2O$ and $CuSO_4$•$5H_2O$ with total 3 mmol were dissolved in 40 mL of distilled water, then 3 mL of cyclohexylamine was added by dropwise under vigorous stirring, and the agitation was kept continuously for 20 min. Finally, the colloid mixture was transferred to 60 mL of Teflon-lined stainless steel autoclave, which was sealed and maintained at 140°C for 12 h. The autoclave cooled down to room temperature naturally, and the sample was filtered and washed with distilled water then ethanol for several times, and dried in vacuum at 60°C for 8 h. By changing Cu/Fe molar ratio, Fe_2O_3, CuO, and CuO/Fe_2O_3 hybrid oxides with Cu/Fe ratios of 1:11, 2:10, 3:9, 4:8, 5:7, 6:6, 9:3, 10:2 and 11:1 were synthesized, respectively.

2.3. Characterization of the samples

The phases analysis of the as-synthesized samples was carried out on a Philips X'Pert PROSUPER X-ray diffraction (XRD) with Cu Kα radiation (λ=0.154178 nm), using an operation voltage and current of 40 kV and 50 mA. The FE-SEM images were collected on a JEOL-6300F Field-emission scanning electron microscopy (FE-SEM) with accelerating voltage of 15kV. The TEM images were collected on a Hitachi Model H-800 transmission electron microscope, using an accelerating voltage of 200 kV. The high resolution transmission electron microscopy (HR-TEM) image was detected by JEOL-2010 high resolution transmission electron microscopy, with an accelerating voltage of 200 kV. X-ray photoelectron spectroscopic (XPS) measurements were performed with an ESCALAB 250 VG Lited XPS operated at 15 kV (hv = 1486.6 eV).

2.4. Electrocatalysys experiments

Electrocatalytic measurements were performed on the LK 98 microcomputer-based electrochemical system (Tianjin Lanlike Chemical and Electron High Technology Co., Ltd., Tianjin in China). Typically, a three-electrode single compartment cell was used for cyclic voltammetry. A GCE (3.7 mm diameter) was used as working electrode and a platinum plate (Pt) as counter electrode and a Ag/AgC1 electrode as reference electrode. Before each determination, the surface of a GCE was polished carefully on an abrasive paper first, further polished with 0.3 and 0.05 μm α-Al_2O_3 paste in turn, and then rinsed completely with doubly distilled water and absolute alcohol. 20 mg of sample was dispersed in 4 mL of doubly distilled water under ultrasonication conditions to obtain a suspension solution. Of the suspension solution, 50 μL was taken out and trickled on the surface of carbon of the GCE. After being dried automatically in air, a modified GCE was prepared and used directly for electrochemical measurement.

2.5. Photocatalytic properties

Photocatalytic degradation experiment was performed in a self-prepared reactor. 0.10 g of photocatalyst was dispersed in a 250 mL of beaker containing 200 mL of wastewater (initial pollutant concentration was fixed at 20 mg L^{-1}) under ultrasonication conditions for 30 min by keeping the reactor from irradiation of light. A 200 W incandescent lamp used as irradiating source, and the vertical distance between the level of the solution and the horizontal plane of the lamp was fixed at 10 cm. As soon as the irradiation began, 0.5 mL of oxydol solution (30%, m/v) was added, and the wastewater was stirred vigorously. At an interval of 20 min, 3 mL of solution was taken out and centrifuged for analytical determination. The absorbance of the sample was determined on a UV-Vis absorption photometer (T6, Puxitongyong analytic apparatus Ltd. Inc., Beijing, China) worked at 464 nm. The concentration of pollutant in wastewater was obtained according to a calibration curve. The degradation rate of the pollutant (η) was calculated as the following equation:

$$\eta = \frac{C_0 - C_t}{C_0} \times 100$$

where C_0 is the initial concentration of pollutant; C_t concentration of pollutant at any time "t".

3. Results and discussion

3.1. Phase and morphology of the samples

Fig. 1 shows the XRD patterns of Fe_2O_3 and CuO/Fe_2O_3 hybrid oxides with Cu/Fe molar ratios. According to curve a, without addition of Cu^{2+}, pure Fe_2O_3 phase appeared and its characteristic diffraction peaks were in good agreement with monoclinic α-Fe_2O_3 (JCPDS

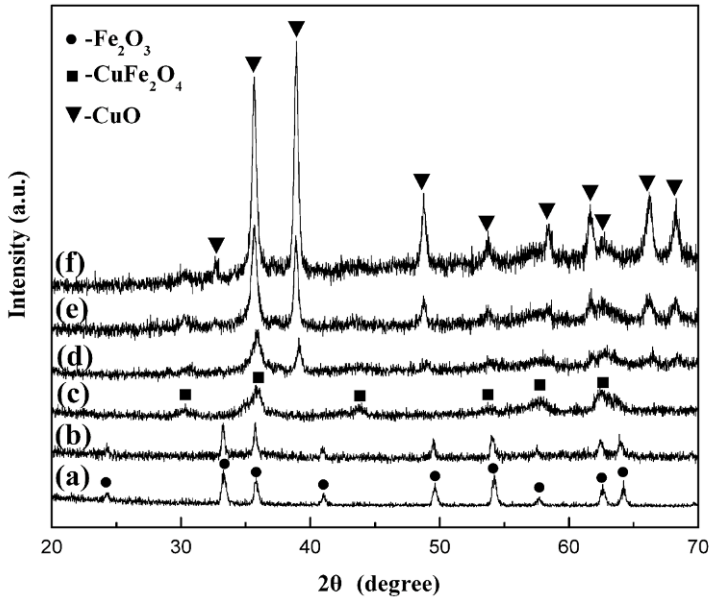

Figure 1. XRD patterns of Fe_2O_3 (a) and CuO/Fe_2O_3 composite oxides with different molar ratios: (b) 2:10, (c) 4:8, (d) 6:6, (e) 8:4 and (f) 10:2.

File No. 89-0597). From curve b, the characteristic diffraction peaks of CuO/Fe_2O_3 hybrid with Cu/Fe ratio of 2:10 also was due to monoclinic α-Fe_2O_3, and no characteristic diffraction peak of CuO was observed (curve b). This may be attributed to the formation of spinel $CuFe_2O_4$ phase with weak diffraction peaks which are shielded by the stronger ones of α-Fe_2O_3 phase. By increasing Cu/Fe ratio to 4:8, neither α-Fe_2O_3 nor CuO phase were detected, but $CuFe_2O_4$ phase with spinel structure appeared (curve c). It is well known that Fe_3O_4 has an inverse-spinel structure, and half Fe^{3+} ions occupy tetrahedral sites and another half Fe^{3+} ions and total Fe^{2+} ions occupy octahedral sites. Because Cu^{2+} ion possesses the same ionic charge and similar ionic diameter ($D_{Cu(II)}$ = 73 pm and ($D_{Fe(II)}$ = 78 pm) with Fe^{2+} ion, it is reasonable to speculate Cu^{2+} ions replace Fe^{2+} place and form spinel-typed $CuFe_2O_4$. For the hybrid with Cu/Fe ratio of 6:6, both monoclinic CuO and spinel-structured $CuFe_2O_4$ phases was detected (curve d). By further increasing Cu/Fe ratio to 8:4, the characteristic diffraction peaks of the sample were due to monoclinic CuO (JCPDS File No. 05-0661), and $CuFe_2O_4$ phase was so weak that could not be observed (curve e). We deduced that the main reason might be that the crystallinity of CuO was better than that of $CuFe_2O_4$. As Cu/Fe ratio increased to 10:2, only monoclinic CuO phase could be detected (curve f). Without addition of Fe^{3+}, only monoclinic CuO phase was checked, and the corresponding XRD pattern was completely similar to the one of Fe-Cu hybrid oxide with Fe/Cu ratio of 10:2 (the XRD pattern was not given).

The CuO/Fe_2O_3 sample with Cu/Fe ratio of 6:6 was determined by XPS to further verify the composition of the hybrid sample. From the survey XPS spectrum (Fig. 2a), C1s peak located at 284.6 eV, and except C, Fe, Cu and O, no peaks owning to other elements could be observed, which indicated that the sample was consisted of copper and iron oxides. The high-resolution XPS spectra of Fe2p, Cu2p and O1s of the sample are shown in Fig. 2b, c. and d, respectively. From Fig. 2b, two obvious peaks located at binding energies of about 711.5 eV for $Fe2p_{3/2}$ and 725.5 eV for $Fe2p_{1/2}$, which were well consistent with the values reported in the literatures [29,30]. In Fig. 2c, two peaks at binding energies of approximate 932.2 and 952.5 eV were attributed to $Cu2p_{3/2}$ and $Cu2p_{1/2}$, respectively, which were consistent with the literature values [31,32]. The gap between the $Cu2p_{3/2}$ and $Cu2p_{1/2}$ lever was 20.1 eV, which was closed to the same value in the standard spectrum of CuO. Additionally, the clear peaks of Cu2p indicated that the existence of Cu^{2+} in the composite sample. Furthermore, the existence of the strong shake-up characteristics for Cu(2p) locating at binding energy in the range from 933.5 to 945 eV ruled out the possibility of the presence of Cu_2O phase in essence. From Fig. 2d, the broaden peaks at binding energy of 529.8 eV were due to O1s. Based on the XPS data, the sample with Cu/Fe ratio of 6:6 was confirmed as CuO/Fe_2O_3 hybrid oxides.

The morphologies of the samples were determined by TEM, HR-TEM and FE-SEM. The results are shown in Fig. 3. From Fig. 3a, α-Fe_2O_3 sample was nanoparticles with mean size of around 100 nm and in good dispersion, for no obvious aggregation could be observed. From

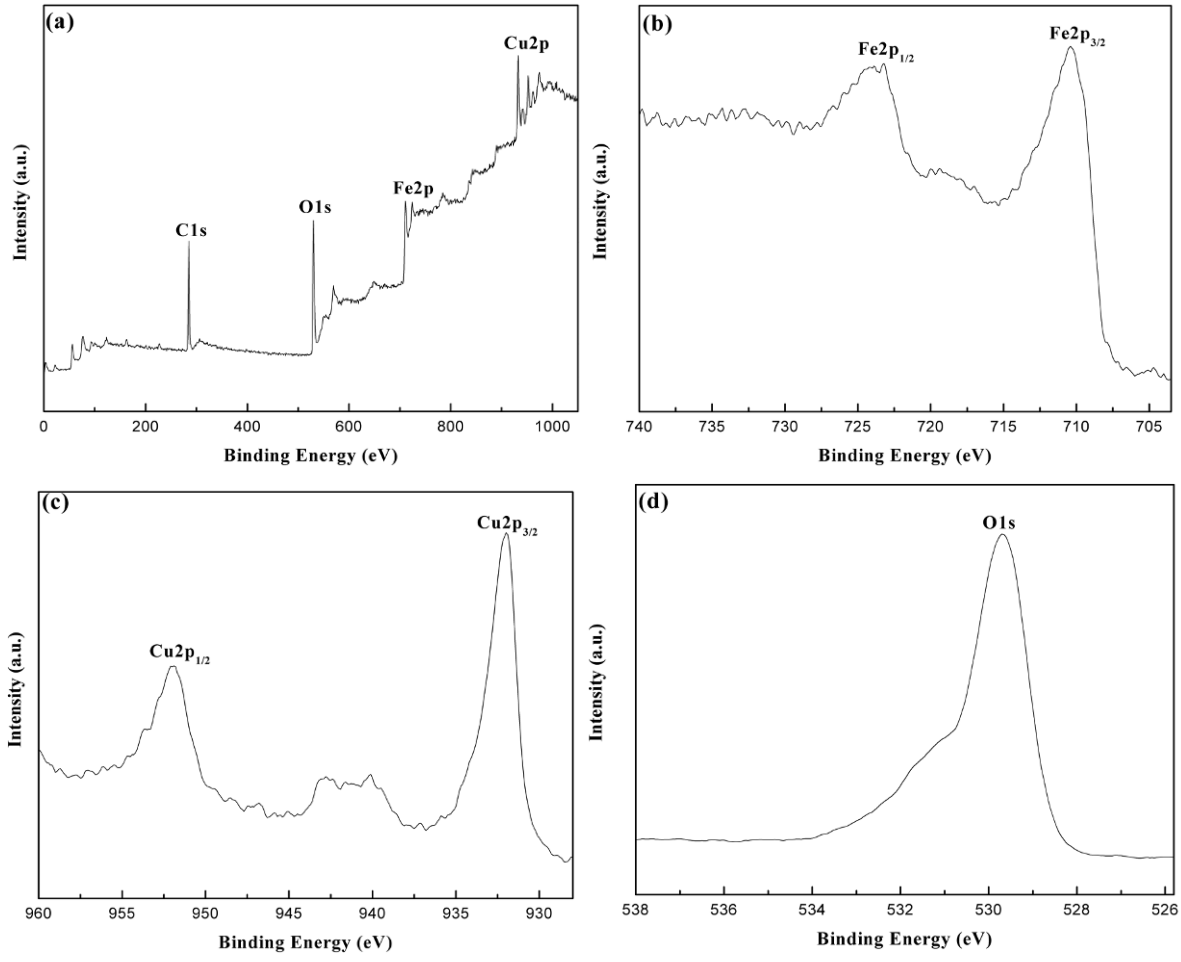

Figure 2. XPS spectra of CuO/Fe_2O_3 sample with Cu/Fe ratio of 6:6

Fig. 3b, the morphology of the sample with Cu/Fe ratio of 1:11 was similar to that of *α*-Fe_2O_3, but its size increased clearly (with a mean size of about 150 nm). In addition, a small amount of cube-like crystals appeared. By increasing Cu/Fe ratio to 2:10, the sample displayed mainly cube-like shape, and its size was closed to that of the sample with Cu/Fe ratio of 1:11 (Fig. 3c). From the overall morphology of FE-SEM image (Fig. 3d), the sample with Cu/Fe ratio of 1:11 mainly displayed cube-like shape in a large scale. From the low-magnification FE-SEM image, it can be seen that its size was not uniform (Fig. 3e). By further increasing Cu/Fe ratio to 3:9, however, the size of the sample decreased markedly and its morphology changed evidently (it was mainly consisted of irregular cubes and nanoparticles), and the regular cube-like crystals almost disappeared (Fig. 3f). From Fig. 3g, one can see that the sample with Cu/Fe ratio of 4:8 was composed of uniform nanoparticles with mean size of around 20 nm. By further increasing the Cu/Fe ratio to 6:6, the sample was also consisted of nanoparticles but its mean size decreased to about 15 nm (Fig. 3h). As Cu/Fe ratio increased to 9:3, there were a few nanorods in the sample and a great deal of nanoparticles placed between the rods, furthermore, a small amount of large-sized particles appeared (Fig. 3i). From Fig. 3j, the morphology of the sample with Cu/Fe ratio of 10:2 was similar to that of the one with Cu/Fe ratio of 9:3, but the nanorods grew longer. In the sample with Cu/Fe ratio of 11:1, the amount of rod-like products increased. Intriguingly, a few products with plane-like shape assembling with nanorods appeared, and the amount of nanoparticles decreased evidently (Figs. 3k and 3*l*). Without the addition of Fe^{3+}, the pure CuO sample exhibited a special gear-like 3-demensional structure, in which the sample could consist of a few CuO nanosheets or nanorods (Fig. 3m). Fig. 3n displays a typical HR-TEM image of CuO/Fe_2O_3 with Cu/Fe ratio of 4:8. From Fig. 3n, the lattice fringes of the sample were clear, verifying good crystallinity.

From Fig. 3, by changing Cu/Fe molar ratio in the range from 0:12 to 12:0, it can be seen that the morphologies of Fe_2O_3, CuO/Fe_2O_3 hybrids and

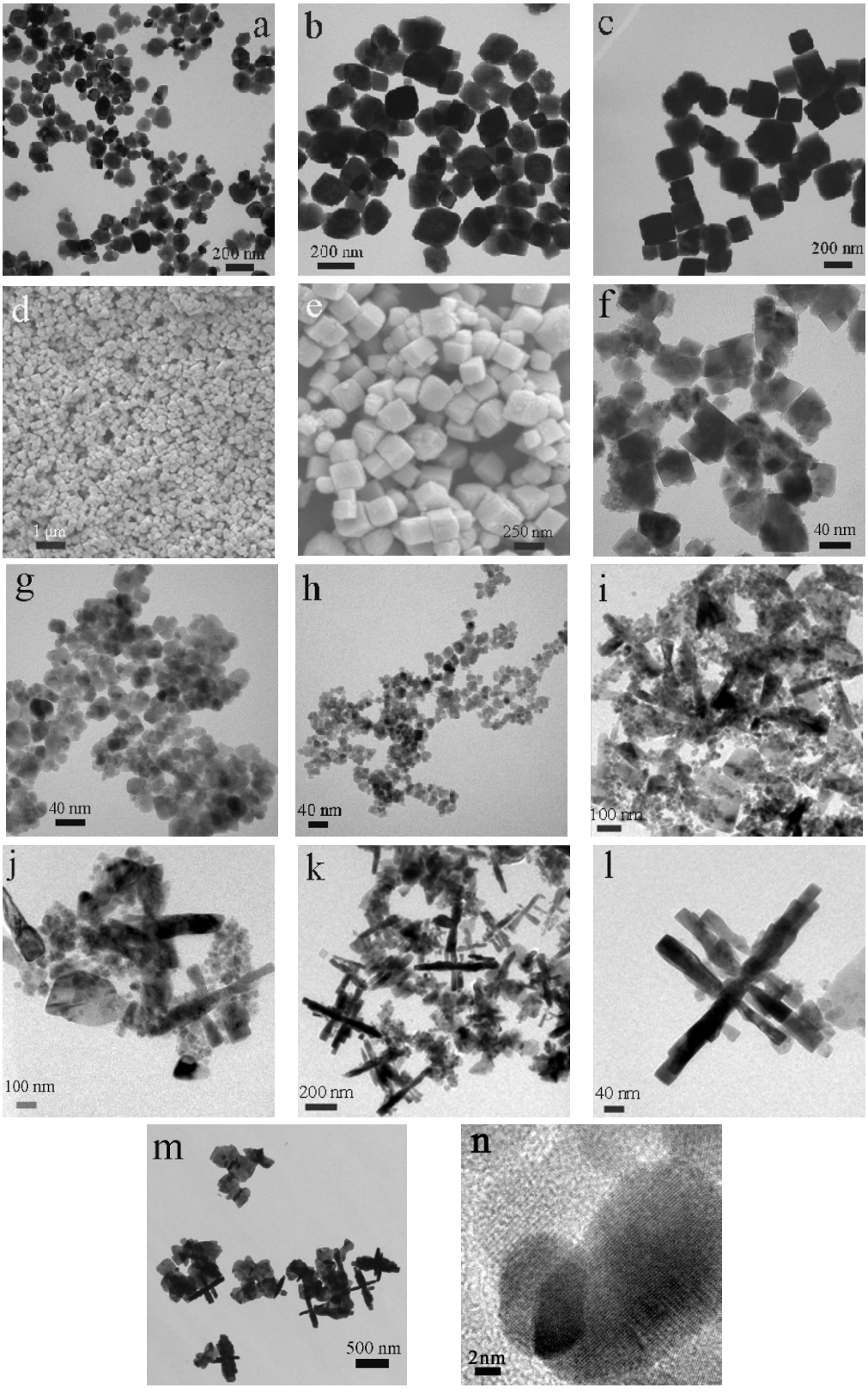

Figure 3. TEM images of (a) Fe_2O_3, CuO/Fe_2O_3 samples with Cu/Fe ratio of (b) 1:11, (c) 2:10, (f) 3:9, (g) 4:8, (h) 6:6, (i) 9:3, (j) 10:2, (k) and (l) 11:1, and of (m) CuO. FE-SEM images of (d) and (e) CuO/Fe_2O_3 sample with Cu/Fe ratio of 2:10. HR-TEM image of (n) CuO/Fe_2O_3 sample with Cu/Fe molar ratio of 4:8.

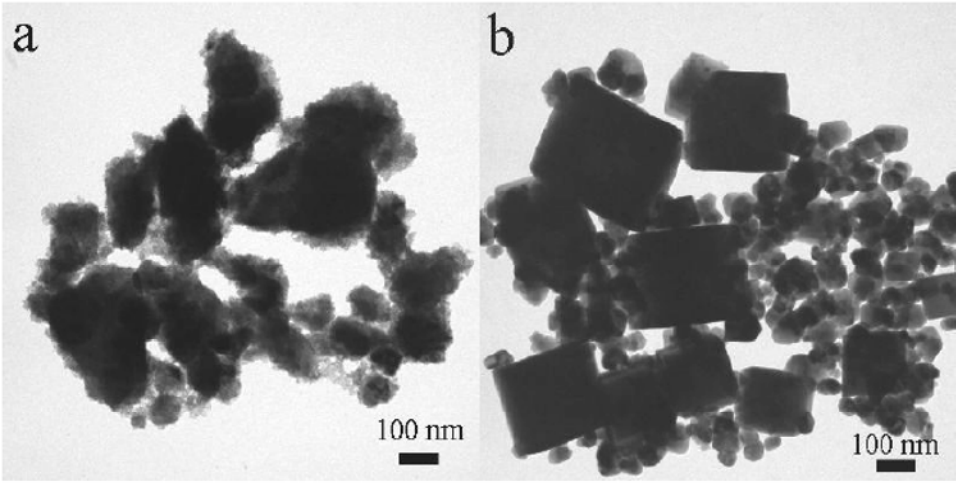

Figure 4. TEM images of CuO/Fe_2O_3 samples with Cu/Fe ratio of 2:10 prepared at (a) 100 and (b) 180°C, respectively.

CuO samples changed markedly. Obviously, the morphologies of samples were mainly dependent on their compositions. Herein, the conformation mechanism of Fe_2O_3, CuO/Fe_2O_3, and CuO samples can be discussed. With addition of cyclohexylamine, the organic amine reacted with water and released hydroxyl ion (OH^-), which provided a alkaline media in which M^{n+} (M=Fe, Cu) formed $M(OH)_n$. The surface of $M(OH)_n$ might chemically adsorb organic amine molecules by hydrogen bonding between the N-H group of the amine and O-H of $M(OH)_n$ [33]. The binding force between $M(OH)_n$ and organic amine generally was so strong that the nanocrystals were highly stabilized, which prevented crystal growth from further occurring. Consequently, the nanocrystals could restructure by organic amine at the interfaces between the hybrid building blocks, leading to the Fe_2O_3/CuO samples with different Fe/Cu ratios displayed different morphologies. Additionally, because the solubility of $Fe(OH)_3$ ($K_{sp}(Fe(OH)_3)= 4\times10^{-38}$) was much lower than that of $Cu(OH)_2$ ($K_{sp}(Cu(OH)_2)=2.2\times10^{-20}$), the formation speed of nuclei of $Fe(OH)_3$ was faster than the one of $Cu(OH)_2$, which caused preparation of Fe_2O_3 to be easier than CuO. As a result, the Fe_2O_3 was mainly composed of nanoparticles, but CuO had a special gear-like 3-demensional structure.

Experiments were performed to investigate the effect of reaction temperature on the morphology of the samples exemplifying CuO/Fe_2O_3 hybrid oxide with Cu/Fe ratio of 2:10. The controlled experiments were performed at 100 and 180°C, respectively. The corresponding TEM images are shown in Fig. 4. The sample synthesized at 100°C displayed amorphous particles, and no cube-like product was detected (Fig. 4a), which was indicative of that the sample could not grow completely under 100°C. The sample prepared at 180°C was composed both of cubes and nanoparticles, furthermore the cubes and nanoparticles separated clearly (Fig. 4b), which verified that the formation speed of CuO and Fe_2O_3 nucleus was too fast, which was not favorable to grow cubic-like CuO/Fe_2O_3. By comparing Fig. 4 to Fig. 3c, the favorable temperature for synthesizing cube-like CuO/Fe_2O_3 with Cu/Fe ratio of 2:10 should be controlled at 140°C or so. Additionally, the effect of cyclohexylamine volume on the morphology of CuO/Fe_2O_3 hybrid with Cu/Fe ratio of 2:10 was investigated. With 1.25 mL of cyclohexylamine, the sample was composed of both nanoparticles and nanocubes, certifying the incomplete growth (Fig. 5a). By increasing cyclohexylamine volume to 2.50 mL, the sample almost exhibited cube-like morphology (Fig. 5b). Further increasing cyclohexylamine volume to 3.75 and 5.00 mL, the samples all exhibited cube-like shape, furthermore they were comparatively uniform (shown in Figs. 5c and 5d, respectively). Thus, based on the controlled experiments, the suitable cyclohexylamine volume was no less than 2.50 mL for synthesizing cube-like CuO/Fe_2O_3 sample in uniform shape.

3.2. Electrocatalytic property and electrochemical impedance of the samples

The electrocatalytic performances of CuO/Fe_2O_3 samples with low Cu/Fe ratios modified on a GCE for *p*-nitrophenol reduction in a basic solution were investigated. The result shows in Fig. 6. From Fig. 6, a bare GCE displayed weak catalytic activity, for its reduction peak current was low and was only 40 μA at peak potential of -1.044 V (curve 1). When the GCE modified with pure Fe_2O_3 and CuO/Fe_2O_3 with Cu/Fe ratio of 1:11, 2:10, 3:9, 4:8, 5:7 and 6:6, respectively, were used in turn, the corresponding reduction peak potential and peak current were displayed in Table 1.

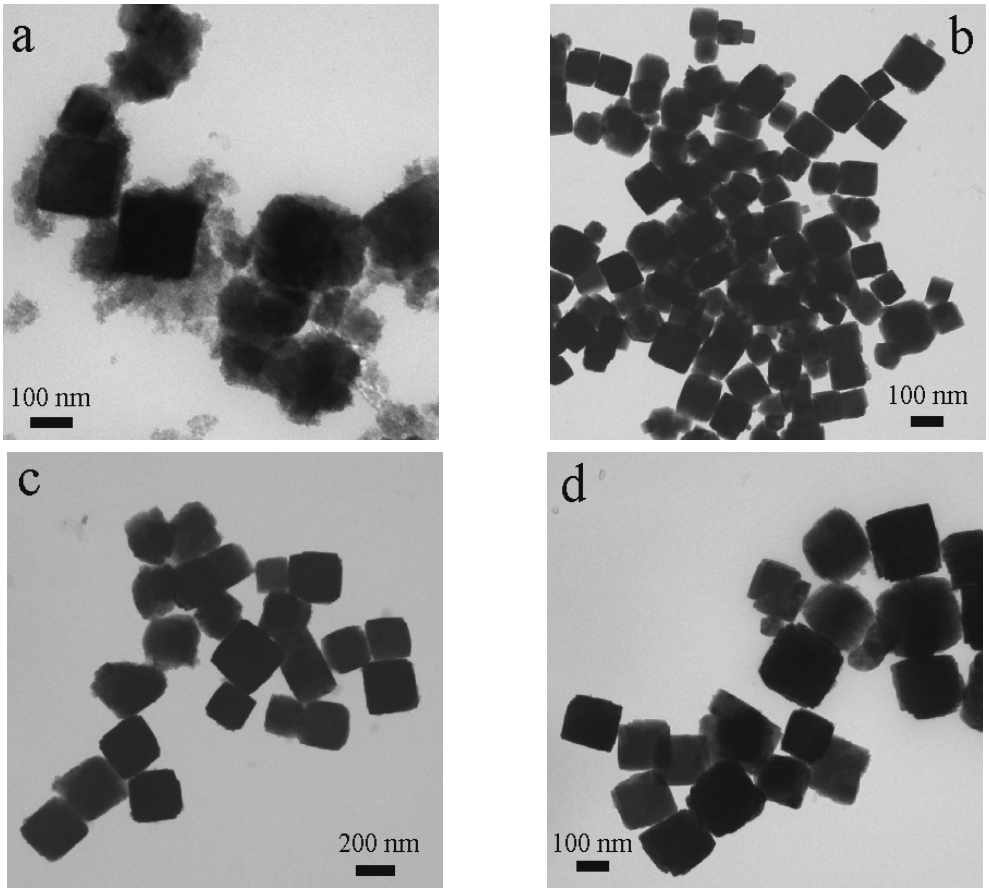

Figure 5. TEM images of CuO/Fe_2O_3 samples with Cu/Fe ratio of 2:10 prepared with addition of (a) 1.25, (b) 2.50, (c) 3.75 and (d) 5.00 mL of cyclohexylamine.

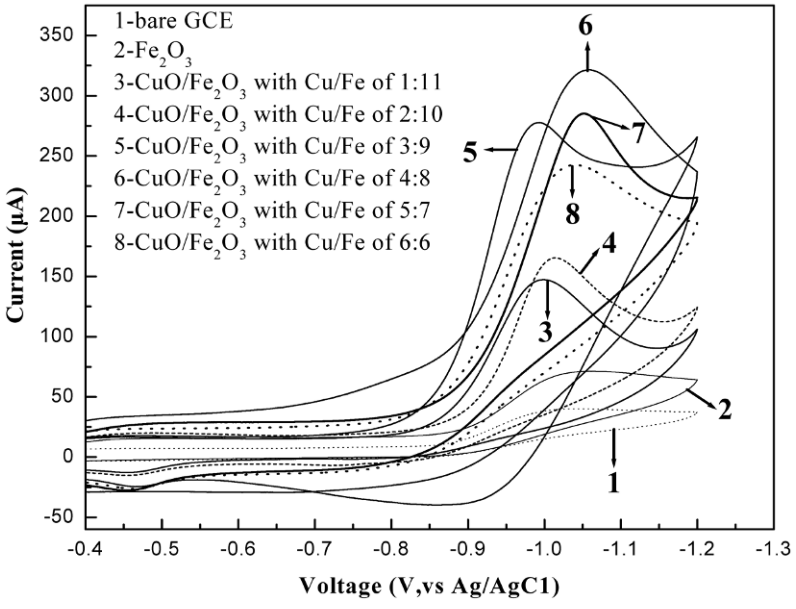

Figure 6. Cyclic voltammorgrams of a bare GCE and the one modified with Fe_2O_3 and CuO/Fe_2O_3 with Cu/Fe ratios of 1:11, 2:10, 3:9, 4:8, 5:7 and 6:6 respectively in 1.0 M sodium hydroxide +1.0 mM p-nitrophenol (scan rate 0.02 V s^{-1}).

Table 1. I_{pc} versus peak potential with samples for p-nitrophenol reduction in a basic solution.

	A bare CE 0	Cu/Fe 1:11	Cu/Fe 2:10	Cu/Fe 3:9	Cu/Fe 4:8	Cu/Fe 5:7	Cu/Fe 6:6	Cu/Fe
Peak voltage/V	-1.044	-1.047	-0.994	-1.010	-0.987	-1.050	-1.050	-1.033
Peak current/μA	40	71	147	165	277	321	285	242

Table 2. Effect of irradiation time on the degradation rate of methyl orange without addition of H_2O_2 (catalyst: CuO/Fe_2O_3 with Cu/Fe ratio of 8:4).

Irradiation time (min)	20	40	60	80	100	120
Degradation rate	7.6	8.5	9.2	9.8	10.3	10.6

From Table 1, in comparison with a bare GCE, their reduction peak potentials almost kept invariable, but the corresponding peak currents clearly increased, and were 1.8, 3.7, 4.1, 6.9, 8.0, 7.1 and 6.0 times bigger than that with a bare GCE. In a whole, the electrocatalytic activity of CuO/Fe_2O_3 sample increased first and then decreased as Cu/Fe molar ratio of the sample varied in the range from 1:11 to 6:6. Among the hybrids, the one with Cu/Fe ratio of 4:8 exhibited the highest catalytic activity. Based on Fig. 3, the size of the sample was smallest and might have a larger special surface area and be favorable for the catalytic enhancement. Additionally, according to the XRD analysis, the CuO/Fe_2O_3 sample with Cu/Fe ratio of 4:8 demonstrated a spinel-typed structure, in which O^{2-} anions piled at face-center cube, the larger sized Cu^{2+} ions occupied 1/8 tetrahedral sites and the smaller sized Fe^{3+} ions occupied 1/2 octahedral sites. The special structure could be favorable to electron transportation between Cu^{2+} and Fe^{3+} ions. Hence, the corresponding $CuFe_2O_4$ sample showed higher electrocatalytic activity.

From Fig. 6, it also can be seen that CuO/Fe_2O_3 sample even with Cu/Fe ratio of 1:11 showed a higher activity than pure Fe_2O_3, for the peak current was two times bigger than that of α-Fe_2O_3, which indicated that addition of Cu^{2+} could effectively enhance the electrocatalytic activity. In the experimental, the CuO/Fe_2O_3 samples with higher Cu/Fe molar ratios also were investigated, and the results showed that the stability of the modified electrode was quite weak and its reproducibility was very bad, for the peak current decreased sharply and the reduction peak location shifted heavily in the second scanning even using a same scan velocity. The experiments showed that it was suitable for CuO/Fe_2O_3 hybrid oxides with low Cu/Fe ratios to act as electrocatalyst modified on a GCE for *p*-nitrophenol reduction in a basic solution.

In 0.1 mol L^{-1} KCl solution containing each 0.005 mol L^{-1} $K_3[Fe(CN)_6]$ and $K_4[Fe(CN)_6]$, the impedance properties of GCE and the GCE modified with CuO/Fe_2O_3 with Cu/Fe ratio of 2:10 and 4:8 were investigated. The results are shown in Fig. 7. From Fig. 7, the alternating-current impedance of the GCE modified with CuO/Fe_2O_3 samples with Cu/Fe ratio of 2:10 and 4:8 approximately displayed half-circled shape in high frequency. However, the radius of the alternating-current impedance of the hybrid with Cu/Fe ratio of 4:8 was smaller clearly than that of the hybrid with Cu/Fe ratio of 2:10, which indicates that the impedance of the GCE with hybrid with Cu/Fe ratio of 4:8 was lower than that of the GCE with the hybrid with Cu/Fe ratio of 2:10. The results verified that the GCE modified with smaller sized CuO/Fe_2O_3 with Cu/Fe ratio of 4:8 had a larger specific surface area, and there was a great deal of gaps in the membranous layer of modified GCE, leading to $K_3[Fe(CN)_6]/K_4[Fe(CN)_6]$ reached the surface of the GCE via the gaps and caused electronic transferring easily. From Fig. 7, it also verified that CuO/Fe_2O_3 samples were successfully modified on the GCE.

3.3. Photocatalytic property of the samples

Both Fe_2O_3 and CuO are excellent semiconductors. Fe_2O_3 is a typical *n*-type semiconductor (E_g=2.1 eV) while CuO is a *p*-type one (E_g=1.21 eV). So a p-n junction between CuO and Fe_2O_3 can form, leading to enhanced visible-light photocatalytic activity of the hybrid oxide catalyst [34]. In the work, CuO/Fe_2O_3 hybrid oxides and pure CuO were used as photocatalysts for degradation of methyl orange with the assistance of oxydol under irradiation of visible light. The results show in Fig. 8. From Fig. 8, the degradation of methyl orange increased with prolonging irradiation time. It also can be seen from Fig. 8 that the sample with different Cu/Fe molar ratio displayed different photocatalytic activity. After being irradiated for 120 min, degradation rate reached 77.5, 85.6, 92.5, 97.5, 96.3 and 91.7% when CuO/Fe_2O_3 hybrid oxides with Cu/Fe ratios of 2:10, 4:8, 6:6, 8:4, 10:2 and CuO were used as catalysts, respectively.

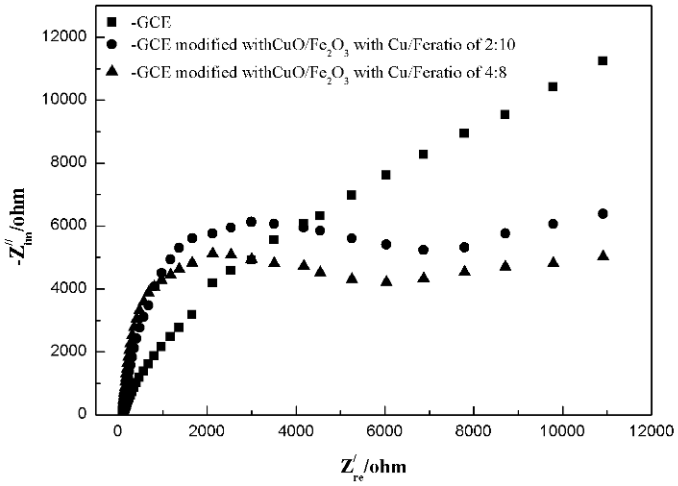

Figure 7. Electrochemical impedance spectra obtained at bare GCE (■), GCE modified with CuO/Fe_2O_3 with Cu/Fe ratio of 2:10 (●), and 4:8 (▲) in 0.1 mol L^{-1} KCl containing 0.005 mol L^{-1} $K_3[Fe(CN)_6]/K_4[Fe(CN)_6]$ (1:1).

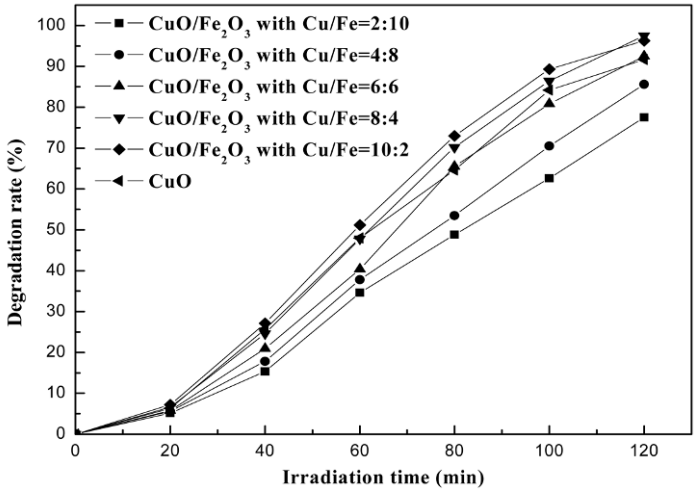

Figure 8. Effect of irradiation time on the degradation rate of methyl orange using CuO/Fe_2O_3 samples with different Cu/Fe ratios (the input amount of catalyst was 0.5 g L^{-1}, initial concentration of methyl orange was 20 mg L^{-1}).

The results indicated that the catalytic activity of CuO/Fe_2O_3 sample increased with increasing of Cu/Fe ratio, which might be attributed to a lower energy gap of CuO than that of Fe_2O_3, for CuO could utilize visible more effectively. However, the pure CuO did not exhibit the highest catalytic activity as expected, indicating the hybrid catalyst might have a synergic effect or the catalytic activity was influenced by not only the energy gap but also the morphology and structure of the catalyst. Among the catalysts, the sample with Cu/Fe ratio of 8:4 revealed the highest catalytic activity. As the sample with higher Cu/Fe molar ratio was used, its catalytic activity had a slight decrease.

It is well known that degradation of organic pollutant is strongly dependent on the concentration of hydroxyl radical (HO·) in solution and the positive hole (h_{vb}^+) number in the semiconductor, which are produced by excitation under irradiation of light. Both HO· and h_{vb}^+ have higher energy and can oxidize organic pollutants into inorganic materials, as a result the pollutants can be degraded effectively [35]. To study the mechanism of photocatalytic degradation of methyl orange, the controlled experiments were performed using CuO/Fe_2O_3 sample with Cu/Fe ratio of 8:4 as catalyst without addition of H_2O_2. The results show in Table 2. From Table 2, as the solution with 20 mg L^{-1} of methyl orange was irradiated for 120 min, its degradation rate was very low and only 10.6%, which indicated addition of H_2O_2 played a significant role on methyl orange degradation. Without addition of H_2O_2, the HO· number in solution was very low for HO· radicals were difficult to produce under irradiation of visible light with low energy. Additionally, the other comparison experiments were carried out as

Table 3. Effect of irradiation time on the degradation rate of methyl orange with addition of H_2O_2 but no catalyst.

Irradiation time (min)	20	40	60	80	100	120
Degradation rate	4.2	5.7	6.4	6.8	7.4	7.5

the solution was irradiated by visible light with addition H_2O_2 but without CuO/Fe_2O_3. The results are displayed in Table 3. According to Table 3, without catalyst, degradation rate of methyl orange was even much lower, and its value was only 7.5% by irradiating for 120 min. According to the comparison experiments, it could be deduced that hydroxyl radicals (HO·) were produced mainly from H_2O_2 by catalysis of CuO/Fe_2O_3 sample under irradiation of visible light, which caused *p*-nitrophenol to be oxidized and mineralized into inorganic molecules. So the major methyl orange was degraded by CuO/Fe_2O_3 catalyst with assistance of H_2O_2 under irradiation of visible light. If no H_2O_2 was added, nearly no hydroxyl radical could generate, for water was difficult to decompose even with catalyst under irradiation of visible light. Of course, much hydroxyl radicals could not be produced even with H_2O_2 but without CuO/Fe_2O_3.

4. Conclusions

Fe_2O_3, CuO and CuO/Fe_2O_3 hybrid oxides with different Cu/Fe molar ratios were synthesized via a hydrothermal procedure without any surfactant. The CuO/Fe_2O_3 samples with low Cu/Fe ratios modified on a GCE showed enhanced electrocatalytic activity for *p*-nitrophenol reduction in a basic solution, and that with high Cu/Fe ratios exhibited higher photocatalytic activity for degradation of methyl orange with assistance of oxydol under irradiation of visible light. The as-synthesized CuO/Fe_2O_3 hybrid oxides can possess potential applications in electrocatalysis and photocatalysis fields in the environmental treatment.

References

[1] M. Estrella, L. Barrio, G. Zhou, X. Wang, Q. Wang, W. Wen, J.C. Hanson, A.I. Frenkel, J.A. Rodriguez, J. Phys. Chem. C. 113, 14411 (2009)
[2] D. Li, X. Liu, Q. Zhang, Y. Wang, H. Wan, Catal. Lett. 127, 377 (2009)
[3] L. Zhang, W. Wang, L. Zhou, M. Shang, S. Sun, Appl. Catal. B-Environ. 90, 458 (2009)
[4] W. Li, S. Zheng, B. Cao, S. Ma, J.Nanopart. Res. 13, 2129 (2011)
[5] H. Liu, Y. Wei, P. Li, Y. Zhang, Y. Sunb, Mater. Chem. Phys. 102, 1 (2007)
[6] D.K. Zhong, J. Sun, H. Inumaru, D.R. Gamelin, J. Am. Chem. Soc. 131, 6086 (2009)
[7] K. Pan, H. Ming, H. Yu, Y. Liu, Z. Kang, H. Zhang, S.-T. Lee, Cryst. Res.Technol. 46, 1167 (2011)
[8] K.-S. Jang, J.-D. Kim, J. Nanosci. Nnaotechnol. 11, 4496 (2011)
[9] K. Song, Q. Wang, Q. Liu, H. Zhang, Y. Cheng, Sensors. 11, 485 (2011)
[10] G. Jain, M. Balasubramanian, J.J. Xu, Chem. Mater. 18, 423 (2006)
[11] T. Ben-Moshe, I. Dror, B. Berkowitz, Appl. Catal. B-Environ. 85, 207 (2009)
[12] C. Karunakaran, R. Dhanalakshmi, Cent. Europ. J. Chem. 7, 134 (2009).
[13] C. Karunakaran, P. Anilkumar, Sol. Energ. Mat. Sol. C. 92, 490(2008).
[14] Y. Wang, X. Xia, J. Zhu, Y. Li, X. Wang, X. Hu, Combust. Sci. Technol. 183, 154 (2010)
[15] G. Litt, C. Almquist, Appl. Catal. B: Environ. 90, 10 (2009)
[16] J-L. Cao, Y. Wang, X-L. Yu, S-R. Wang, S-H.Wu, Z-Y. Yuan, Appl. Catal. B: Environ. 79, 26 (2008)
[17] R. Wu, J. Qu, H. Hong, Y. Yu, Chinese Sci. Bull. 48, 2311 (2003)
[18] Z. Yang, Z. Yin, F. Chen, Electrochim. Acta. 56, 1089 (2011)
[19] M. Bomio, P. Lavela, J.L. Tirado, J. Solid State Electrochem. 12, 729 (2008)
[20] I. Nedkov, R.E. Vandenberghe, T. Marinova, P. Thailhades, T. Merodiiska, I. Avramova, Appl. Surf. Sci. 253, 2589 (2006)
[21] X-M. Liu, W-D.Yin, S-B. Miao, B-M. Ji, Mater. Chem. Phys. 113, 518 (2009)
[22] X. Ma, X. Feng, X. He, H. Guo, L. Lü, J. Nat. Gas Chem. 20, 618 (2011)
[23] L.J. Xie, W. Chu, J.H. Sun, P. Wu, D.G. Tong, J. Mater. Sci. 46, 2179 (2011)
[24] P.Sharma, S.K. Sharma, Water Resour. Manage. 26, 4525 (2012)
[25] B-X. Li, Y-Y. Wang, T-F. Wang, Acta Phys-Chim Sin. 25(11), 2366 (2009)

[26] L. Li, Y. Chu, Y. Liu, L. Dong, J. Phys. Chem. C. 111, 2123 (2007)
[27] S. Kakuta, T. Abe, J. Mater. Sci. 44, 2890 (2009)
[28] A. Qurashi, Z. Zhong, M.W. Alam, Solid State Sci. 12, 1516 (2010)
[29] R. Zboril, M. Mashlan, D. Petridis, Chem. Materials.14, 969 (2002)
[30] Z. Xu, J. Yu, Nanoscale. 3, 3138 (2011)
[31] R.A. Zarate, F. Hevia, S. Fuentes, V.M. Fuenzalida, A. Zúñiga, J. Solid State Chem. 180, 1464 (2007)
[32] J. Yu, J. Ran, Energ. Environ. Sci. 4, 1364 (2011)
[33] H. Cölfen, S. Mann, Angew. Chem. Int. Ed. 42, 2350 (2003)
[34] G. Dai, J. Yu, G. Liu, J. Phys. Chem. C 115, 7339 (2011)
[35] Q.J. Xiang, J.G. Yu, P.K. Wong, J. Colloid Interf. Sci. 357, 163 (2011)